

<https://doi.org/10.1038/s41612-025-00929-w>

# How much do atmospheric depressions and Mongolian cyclones contribute to spring dust activities in East Asia?

Feifei Mu <sup>1</sup>✉ & Stephanie Fiedler <sup>1,2,3</sup>

Severe East Asian dust storms occur in spring due to dust-emitting winds in the Gobi Desert associated with Mongolian cyclones. The present study performs the first quantitative assessment of the contributions of Mongolian cyclones to springtime dust activity in East Asia, based on multiple reanalyses and observational datasets for 2001–2022. Atmospheric depressions dominate dust activities in Northern China, explaining ~90–92% of the total dust emissions in the Gobi Desert and ~88–93% of the dust aerosol optical depth ( $\tau$ ) downwind, depending on the dataset. Mongolian cyclones, defined as long-living and mobile atmospheric depressions, explain almost half (~34–47%) of the Gobi's total dust emissions and  $\tau$  downwind, and are the primary driver of high-impact dust storms. The number of Mongolian cyclones, along with the dust activity, has decreased since 2001, with a spatial pattern of the dust emission trend that is consistent with the northward shift of cyclone tracks.

Natural aerosol emissions of desert-dust particles have a profound impact on climate, air quality, and human health<sup>1–3</sup>. Originating mainly from the Taklamakan Desert and the Gobi Desert, East Asia contributes approximately 11% of the global dust loading<sup>4</sup>. Dust aerosols affect the climate through direct effects on radiative transfer, indirect effects by modifying cloud properties, and atmospheric adjustments to the aerosol effects on radiation and clouds<sup>5</sup>. The direct radiative effects of East Asian dust aerosols exhibit a seasonal variation with a maximum in spring, consistent with the high frequency of dust storms<sup>6–8</sup>. Dust aerosols can also act as ice nucleating particles affecting cloud microphysical processes<sup>9</sup>. In addition to climate effects, dust aerosols contribute to poor air quality and impact human health<sup>10,11</sup>. In East Asia, millions of people are affected by the adverse impacts of dust particles from the Gobi and Taklamakan deserts, since the population is exposed to the transported particles during dust outbreaks<sup>12,13</sup>. Multiple case studies suggest that high-impact dust outbreaks in East Asia are driven by extra-tropical cyclones<sup>12,14–32</sup>, but quantitative estimates of the relative contributions of cyclones to the total dust emission and transport in East Asia do not exist.

Investigating the physical mechanisms of dust outbreaks in East Asia can help to improve our understanding of dust aerosols and their changes, which is needed to overcome the persistent uncertainty for simulated dust in climate models that do not reproduce the historical dust trend<sup>33</sup>. East Asia has two major deserts, the Taklamakan and the Gobi. Different meteorological processes contribute to dust emission and affect the subsequent

atmospheric transport in the deserts. The Taklamakan Desert sees frequent dust activity due to relatively small particle sizes and relatively low threshold wind speeds for dust emissions ( $4.4 \pm 0.6 \text{ ms}^{-1}$ )<sup>34–36</sup>. Dust emissions in the Taklamakan Desert are driven by multiple physical mechanisms, e.g., the breakdown of Nocturnal Low-Level Jets and dry convection in heat lows<sup>37,38</sup>. Heat lows are atmospheric depressions that form under the effects of intense solar irradiation<sup>39</sup>. Owing to the topographic barrier at the edges of the Taklamakan Desert, dust aerosols from this desert can only be transported to populated areas in the East when the aerosols reach a height of at least 4 km a.g.l.<sup>40</sup>. Moreover, the eastward transport of the Taklamakan dust can be limited, leading to high PM<sub>10</sub> concentrations and low atmospheric visibility in the West of China, e.g., during the case in mid-March 2021<sup>32</sup>.

Different from the Taklamakan Desert, the Gobi Desert has relatively higher threshold wind speeds for dust emissions ( $9.8 \pm 2.2 \text{ ms}^{-1}$ ) and less frequent dust emissions<sup>34,41</sup>. However, previous studies suggest that super East Asian dust storms are mainly generated from the Gobi Desert due to the passage of Mongolian cyclones<sup>42,43</sup>. Mongolian cyclones form downstream of the Altai-Sayan Mountains<sup>44</sup>, can lead to dust-emitting winds in the Gobi Desert, and allow the subsequent transport of dust-laden air across East Asia<sup>6,12,42</sup>.

Mongolian cyclones in spring as drivers of dust storms in East Asia have been known for some time. Dust emission in the Gobi Desert occurs in the southwestern sector of a Mongolian cyclone<sup>42</sup>. In the southwestern sector, the cold air from higher latitudes is advected in southern directions.

<sup>1</sup>GEOMAR Helmholtz Centre for Ocean Research Kiel, Kiel, Germany. <sup>2</sup>University of Kiel, Kiel, Germany. <sup>3</sup>Present address: Institute of Environmental Physics (IUP), University Heidelberg, Heidelberg, Germany. ✉e-mail: [fmu@geomar.de](mailto:fmu@geomar.de)

The frequency and intensity of Mongolian cyclones decreased in spring from 1979 to 2017<sup>44</sup>. A weakening of the Mongolian cyclone intensity and frequency is reported to be associated with the weakened westerly jet stream and atmospheric baroclinicity in a warming world, leading to a decline of dust storm events in Northern China<sup>45</sup>. Hence, also a decrease in the associated dust storm frequency in spring from 1979 to 2021 is expected, e.g., seen in in-situ observations of atmospheric visibility and ambient PM<sub>10</sub> concentrations over China<sup>43</sup>. Including also mobile cyclones, atmospheric depressions are reported to be the dominant meteorological process that can generate dust-emitting winds and favor subsequent dust emissions in dust source regions, e.g., North Africa<sup>46</sup>. However, a systematic assessment of the relative contributions of Mongolian cyclones and atmospheric depressions to dust emissions in the Gobi Desert does currently not exist.

Recent studies indicate a decrease in the number of springtime dust storms in Northern China since 2001, at least partly due to the weakening of mean near-surface winds<sup>8,47</sup>. Weakened mean near-surface winds in Northern China are thought to be associated with the decrease in the meridional temperature gradient induced by the faster warming in higher latitudes compared to lower latitudes<sup>48</sup>. Specifically, the enhanced winter-time Arctic amplification may favor the weakened meridional temperature gradient in spring leading to a decrease in the dust storm frequency in Northern China<sup>49</sup>. Despite the mean decrease in dust storm events, exceptionally strong dust storms paired with intense Mongolian cyclones are observed, e.g., in March 2021<sup>32,50–52</sup>. The March 2021 dust storm is attributed to rapid Mongolian cyclogenesis<sup>53</sup>.

Despite the perception of Mongolian cyclones as the primary driver of dust storms in East Asia, a quantitative analysis of their connection using multiple modern datasets to characterize uncertainty in the estimates does currently not exist. We systematically assess the occurrence of springtime dust storms associated with Mongolian cyclones from 2001 to 2022 by combining the results of automatically detected low-pressure systems with different data sets for dust aerosols. The approach allows us to compile the first process-based climatology of observation-based dust aerosol emission and transport for East Asia associated with Mongolian cyclones under present-day conditions. The identification of Mongolian cyclones is based on an automated detection algorithm<sup>54,55</sup> applied to ERA5, the fifth generation of European Centre for Medium-Range Weather Forecasts (ECMWF) reanalysis<sup>56</sup>. The associated dust aerosols are computed based on data sets for dust emission fluxes and for dust aerosol optical depth ( $\tau$ ) taken from Modern-Era Retrospective Analysis for Research and Applications, Version 2 (MERRA-2), Copernicus Atmosphere Monitoring Service (CAMS), and an offline Dust Emission Model (DuEM)<sup>47,57–59</sup>.

## Results

### Climatology and trends of Mongolian cyclones

We first separate the Mongolian cyclones, which are mobile low-pressure systems with a lifetime of at least 24 h, from those identified lows that are short-lived and semi-stationary, here denoted as atmospheric depressions (see “methods”). The mean climatology and trends of Mongolian cyclones in terms of their lifetime, travel distance measured in geographical longitude and latitude, location of cyclogenesis, occurrence frequency, and associated peak winds are shown in Fig. 1. Mongolian cyclones form downstream of the Altai-Sayan Mountains through lee-cyclogenesis (Fig. 1a). The role of blocking of air by the Altai-Sayan Mountains for the formation of Mongolian cyclones in the lee has been shown<sup>60</sup> following the theory of Alpine lee cyclogenesis<sup>61,62</sup>. In the long-term mean,  $7.1 \pm 1.3$  Mongolian cyclones form per spring month (Fig. 1c). The spatial distribution of Mongolian cyclone passages can be inferred from their regional occurrence frequency in Fig. 1b. Most Mongolian cyclones pass the region of 100E°–125E°, and 37N°–53N° (Fig. 1b), motivating the choice of using cyclones passing this region for the analysis of Mongolian cyclone contributions to the dust activity.

Mongolian cyclones have a mean lifetime of ~55 h and travel distances of about 21° in geographical longitude and 5° in geographical latitude over East Asia (Fig. 1d–e). The Mongolian cyclones allow therefore the eastward transport of dust-laden air in East Asia. To measure the intensity of

Mongolian cyclones, the peak winds in a cyclone-affected area with a radius of 5° around the center are analyzed. The mean and maximum peak winds of Mongolian cyclones are higher than in atmospheric depressions in East Asia (Fig. 1f–g). Furthermore, the 5th percentile of the maximum peak winds of Mongolian cyclones ( $\sim 9 \text{ ms}^{-1}$ ; Fig. 1g) is close to previously estimated threshold wind speeds for dust emission in the Gobi Desert ( $9.8 \pm 2.2 \text{ ms}^{-1}$ )<sup>34</sup>, which means that more than 95% of the Mongolian cyclones are strong enough, at least during their peak intensity phases, to potentially emit dust aerosols from the Gobi Desert.

Our analysis shows a negative trend in the occurrence frequency and mean peak winds ( $p < 0.05$ ) of Mongolian cyclones in spring from 2001 to 2022 (Fig. 1c). Similarly, a decrease in the frequency and intensity of spring Mongolian cyclones is observed from 1979 to 2017<sup>44</sup>. The reduced Mongolian cyclone's occurrence frequency and intensity are suspected to be a response to anthropogenic forcing<sup>45</sup>. The increase in surface temperature North of the Gobi Desert has been analyzed in the context of a weakening westerly jet, and a reduced occurrence frequency and intensity of Mongolian cyclones<sup>45</sup>. Nevertheless, strong Mongolian cyclones also occur towards the end of the time series (Fig. 1c), which can cause strong dust outbreaks, e.g., in spring 2021<sup>32,63,64</sup>.

### Co-occurrence of dust and low pressure anomaly

As a first test to what extent Mongolian cyclones coincide with strong dust storms, we present composited anomalies of the mean sea level pressure (SLP) when the spatially averaged hourly dust emission flux in the Gobi Desert exceeds the 95th percentile of the spring climatology for 2001–2022 (Fig. 2). Here we define an extreme dust emission flux in the Gobi Desert, when it is larger than the 95th percentile computed on the spatially averaged hourly dust emission flux. This threshold is deliberately lower compared to the earlier definition<sup>32</sup> to include more dust storms in the statistics. Additionally, we show the daily maximum wind speed at 10 m a.g.l. across the Gobi Desert against the daily maximum peak wind speed of Mongolian cyclones passing D2 to illustrate the impact of Mongolian cyclones on dust-emitting winds in the Gobi Desert (Fig. 2c).

During the extreme dust emission events in the Gobi Desert, an anomalously low mean SLP is seen over southeastern Mongolia and Northern China (D2, as indicated by red box in Fig. 2a), which is the characteristic region for a Mongolian cyclone. A higher threshold, e.g., the 99th percentile, was tested but had no impact on the location of the anomalously low mean sea-level pressure (not shown). It implies that the strongest dust emission events also coincide with the occurrence of a Mongolian cyclone. The location of the pressure anomaly is also right around where Mongolian cyclones are particularly frequently detected by the automated algorithm (compare Figs. 2a, b to 1b), suggesting that the method<sup>54,55</sup> successfully identifies Mongolian cyclones.

The choice of the underlying dust emission data set has a marginal influence on the placement of the co-occurring Mongolian cyclone (compare Fig. 2 a, b), although the magnitudes of the simulated dust emission amounts substantially differ between DuEM and MERRA-2 that use partially different potential dust sources (see next section). The results are broadly consistent with the identification of a similar region for the simultaneous occurrence of Mongolian cyclones and springtime dust storms in previous studies utilizing different data, namely in-situ observations and synoptic analysis of the 850 hPa geopotential heights<sup>43</sup>. Furthermore, dust-emitting wind speeds in the Gobi Desert are positively correlated with the peak wind speeds of Mongolian cyclones passing D2, indicating the successful selection of Mongolian cyclones for Gobi's dust emission (Fig. 2c).

### Associated dust emission amounts

DuEM simulates higher dust emission ( $90.26 \text{ Tg yr}^{-1}$ ) compared to MERRA-2 reanalysis ( $12.96 \text{ Tg yr}^{-1}$ ) by more than a factor of seven in the Gobi Desert (Fig. 3a, b). It is at least in parts explained by the larger number of potential dust sources in DuEM<sup>47</sup> and the use of different dust schemes in DuEM<sup>65</sup> and MERRA-2<sup>66</sup>. However, the relative contributions of

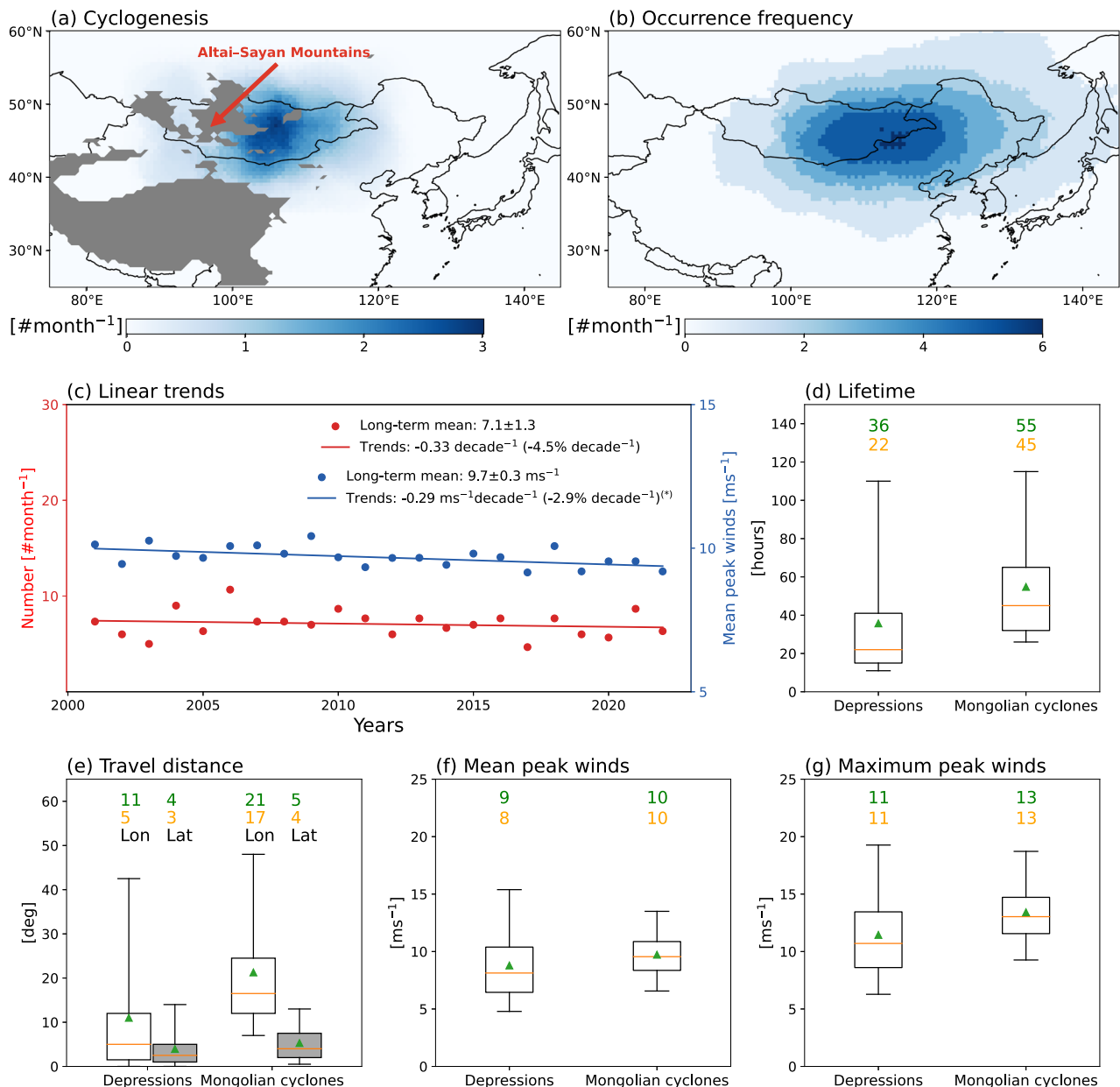


**Fig. 1 | Climatology of Mongolian cyclones for spring 2001–2022.** Shown are spatial patterns of the means for the (a) cyclogenesis and (b) occurrence frequency of all mobile cyclones generated from the downstream of the Altai-Sayan Mountain ( $90^{\circ}\text{E}$ – $120^{\circ}\text{E}$  and  $40^{\circ}\text{N}$ – $53^{\circ}\text{N}$ ), and (c) composite means of the mean peak winds and cyclogenesis per spring and their trends, and (d–g) distributions of lifetime, travel distance in longitude and latitude, mean peak winds, and maximum peak winds of all identified atmospheric depressions and Mongolian cyclones in East Asia. In (d–g),

mean fractions are shown as green triangles and green numbers at the top, medians as orange horizontal lines and orange numbers at the top, gray boxes mark the 25–75% percentiles, and whiskers are the 5–95% percentiles. Gray shading in (a) marks terrain with an elevation of at least 1500 m. Peak winds are the horizontally averaged maximum in 10 m winds that occur within a radius of  $5^{\circ}$  around the center of Mongolian cyclones and atmospheric depressions. (\*) in (c) indicates that the statistical significance exceeds the 95% confidence level.

atmospheric depressions and Mongolian cyclones to dust emissions are remarkably similar in both the dust emission data from DuEM and the MERRA-2 reanalysis in the Gobi Desert (Fig. 4).

Atmospheric depressions in D1 and D2 explain the majority, namely  $\sim 90$ – $92\%$  and  $\sim 72$ – $79\%$ , of the total dust emission flux in the Gobi Desert ( $97^{\circ}\text{E}$ – $112^{\circ}\text{E}$ ,  $38^{\circ}\text{N}$ – $46^{\circ}\text{N}$ , Fig. 4), with the value depending on the dust data. Including also depressions outside of D1 does not strongly affect the contributions of atmospheric depressions to dust emissions in the Gobi Desert.

Mongolian cyclones in D2 contribute  $\sim 39$ – $47\%$  of the total dust emission amount, which increases by less than 10% when all identified Mongolian cyclones across East Asia are included in the statistics (not

shown). The result indicates the importance of atmospheric depressions for dust emissions in the Gobi, with about half of the dust emission associated with Mongolian cyclones (Fig. 4).

We quantitatively estimate the regional contributions of the Mongolian cyclones to the dust emission amounts in the Gobi Desert in spring. To that end, we show the spatial pattern of the ratio of dust emissions associated with atmospheric depressions and Mongolian cyclones in D2, and with atmospheric depressions in D1 relative to the total dust emission amount in spring (Fig. 3). In the Gobi Desert, a regional maximum of 93–100% of total dust emissions are associated with atmospheric depressions in D1 and 47–62% associated with Mongolian cyclones in D2

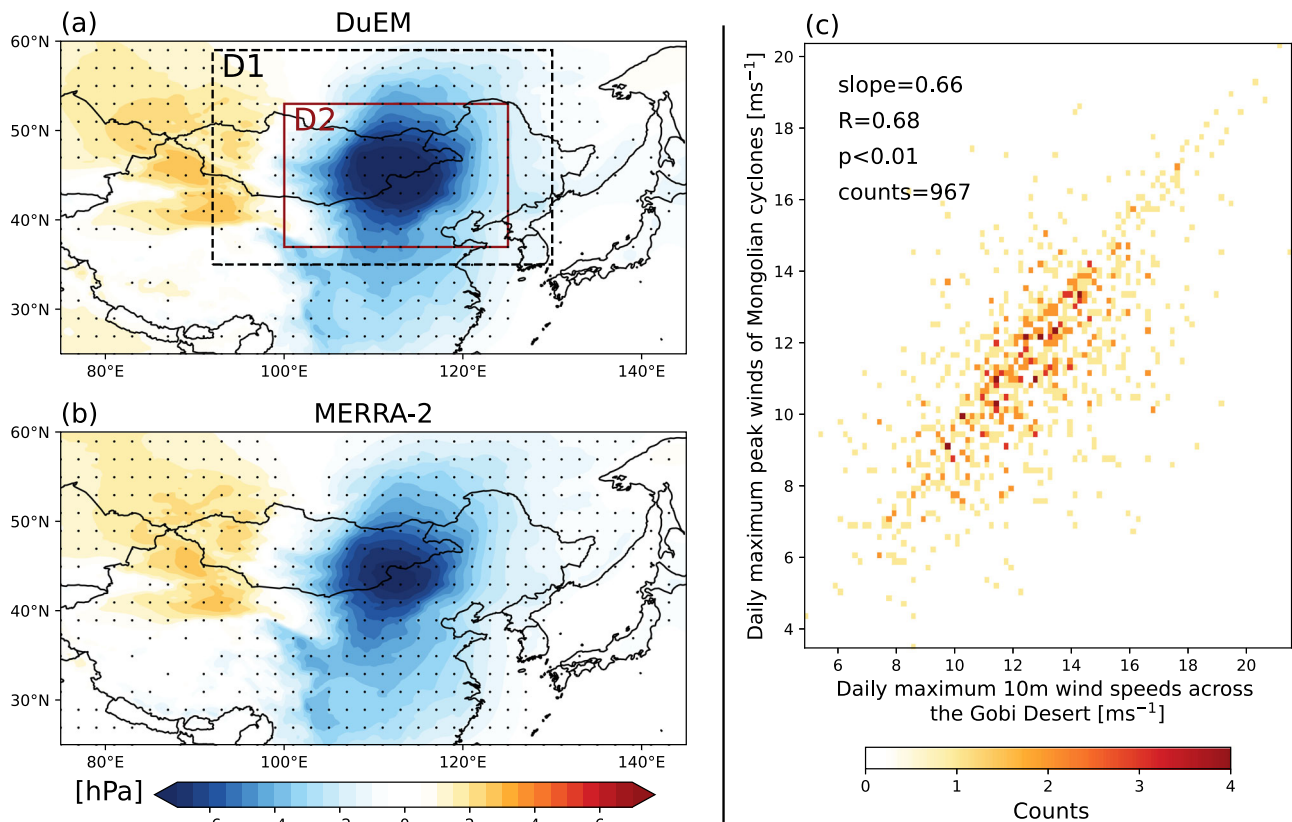


**Fig. 2 | Mean sea level pressure associated with extreme dust emissions in the Gobi Desert.** Shown are composited anomalies of sea level pressure when regional mean dust emission flux in the Gobi Desert (black box in Fig. 3a) exceeds the 95th percentile with data from (a) DuEM and (b) MERRA-2 reanalysis, and (c) scatter plot between daily maximum peak wind speeds of Mongolian cyclones and daily

maximum 10 m wind speeds across the Gobi Desert. Black dots in (a, b) indicate that the circulation changes are significant at the 99% confidence level. The boxes D1 (dashed) and D2 (solid) in (a) are used for the selection of Mongolian cyclones and atmospheric depressions.

(Fig. 3c, d, and g, h). Furthermore, relatively higher contributions of atmospheric depressions and Mongolian cyclones to dust emissions in the region Northern, Eastern, and Southern Gobi Desert are observed in DuEM compared to MERRA-2 (Fig. 3c–h). This is partly due to the high fraction of grassland in that region being included as potential source regions for dust aerosols in DuEM but not in MERRA-2 reanalysis<sup>47</sup>.

### Associated dust aerosol optical depth

The climatology of  $\tau$  and the ratio for  $\tau$  co-occurring with atmospheric depressions and Mongolian cyclones are shown in Fig. 5. Additionally, we show the wind vectors at 700 hPa to illustrate the transport direction of dust aerosol by atmospheric depressions and Mongolian cyclones, as dust aerosols originating from the Gobi Desert are typically transported between 2 and 4 km a.g.l.<sup>40</sup>. Both CAMS and MERRA-2 reanalysis show similar spatial patterns of  $\tau$ , despite the relatively lower  $\tau$  simulated by MERRA-2 in the Gobi Desert and the downwind region (Fig. 5a, b). Similar to dust emissions, atmospheric depressions primarily explain the spatial pattern of  $\tau$ , particularly in Northeast China and East Mongolia (Fig. 5c–f). Averaged over the region (black dashed box in Fig. 5f), ~88–93% of  $\tau$  is associated with atmospheric depressions in D1 and ~67–76% in D2 (Fig. 6), depending on the dust data set. Moreover, CAMS simulates slightly higher contributions of atmospheric depressions and Mongolian cyclones to  $\tau$  than MERRA2 (Figs. 5 and 6).

In Eastern Mongolia and Northeast China, about 34–43% of  $\tau$  is associated with Mongolian cyclones in D2 (Fig. 6). This result is similar but slightly lower compared to an earlier study with different data and methods with namely 58% of the dust aerosols in the Beijing-Tianjin-Hebei (BTH) region associated with the Mongolian plateau based on 15 years of Cloud-Aerosol Lidar with Orthogonal Polarization (CALIOP) observations and

backward trajectories computed with the Hybrid Single Particle Lagrangian Integrated Trajectory Model (HYSPPLIT)<sup>67</sup>. Indeed, dust aerosols are lifted from the Gobi Desert and then transported eastwards with the wind (compare Fig. 3e–h and 5e–h). Consequently, 70–72% and 34–38% (not shown) of  $\tau$  in the BTH region (red dot in Fig. 5f) are associated with atmospheric depressions (including Mongolian cyclones) and Mongolian cyclones alone in D2, respectively.

Both DuEM and MERRA-2 simulate also notably high dust emission fluxes in the Taklamakan Desert (Fig. 3a, b). However, owing to the topography, dust aerosols from this desert can only be transported eastward when they reach an altitude of at least 4 km a.g.l.<sup>40</sup>. Therefore, the Taklamakan Desert contributes less to dust outbreaks compared to the Gobi Desert, indicated by the relatively high  $\tau$  in the Taklamakan desert but not downwind in both CAMS and MERRA-2 reanalysis (Fig. 5a, b). Other driving mechanisms such as the breakdown of low-level jets might also play a role in the regional dust activity of the Taklamakan Desert<sup>37</sup>.

### Trends of dust activity

There is consensus that dust emissions and dust storm frequency in Northern China have decreased, primarily due to the weakening of mean near-surface winds<sup>8,47</sup>. It raises the question of how much of this trend is explained by changes in Mongolian cyclones. To address it, we assess the linear trends in dust emissions and  $\tau$  associated with atmospheric depressions and Mongolian cyclones (Figs. 7a–h and 8a–h). Additionally, we show the relative changes of regionally averaged dust emissions in the Gobi Desert and  $\tau$  downwind (black box in Fig. 8a) in Figs. 7i, j, and 8i, j. The results show negative trends in dust emissions associated with atmospheric depressions and Mongolian cyclones, particularly in the Gobi Desert. Despite the earlier mentioned differences in the absolute magnitudes of dust emission fluxes



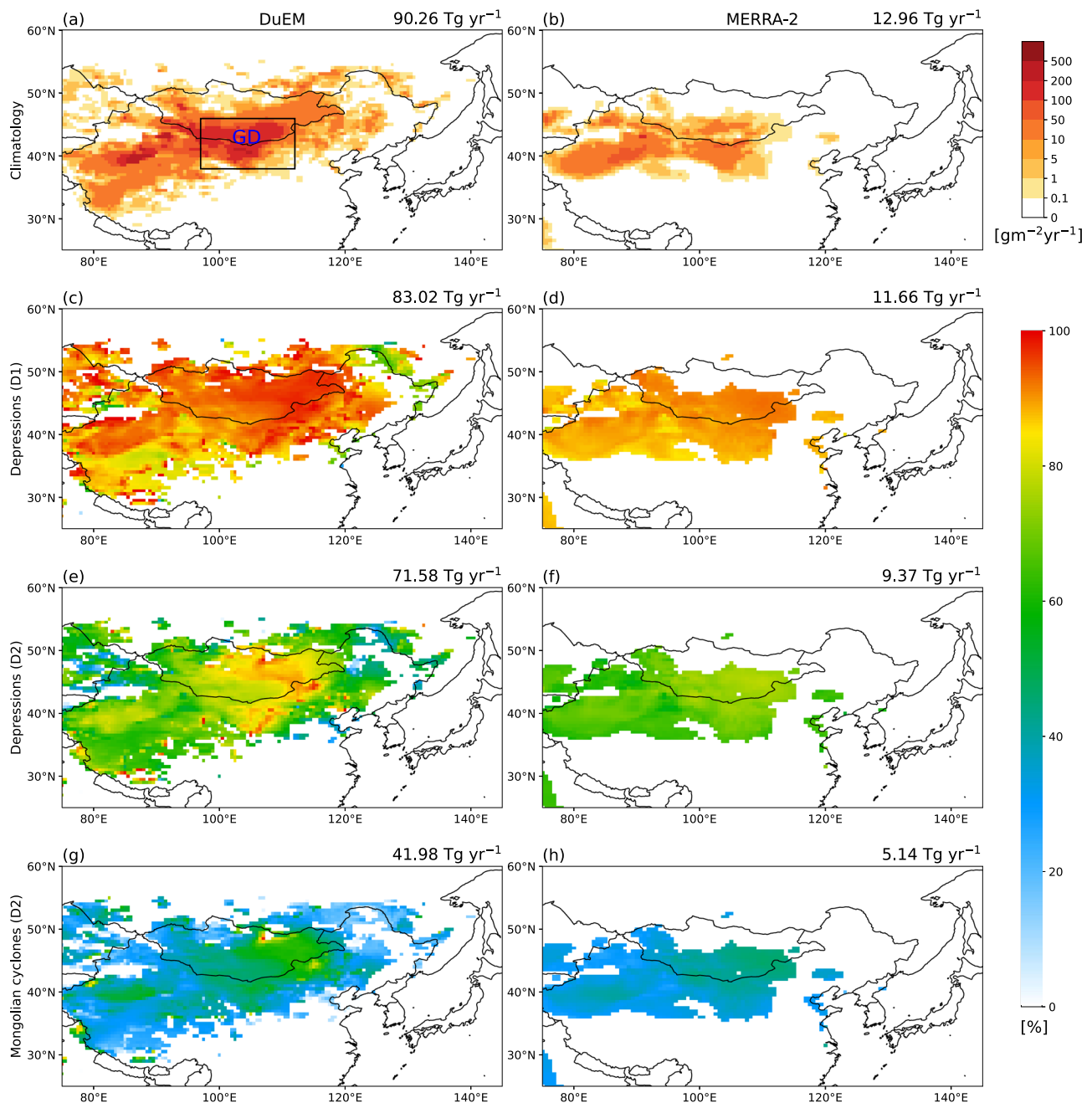


**Fig. 3 | Spatial pattern of the contributions of Mongolian cyclones to springtime dust emissions.** Shown are the mean of the dust emission flux for March to May from (a) DuEM and (b) MERRA-2 reanalysis, (c, d) like (a, b) but for the fraction of total dust emission associated with atmospheric depressions detected in D1, (e, f)

like (c, d) but for atmospheric depression in D2, (g, h) like (e, f) but for Mongolian cyclones in D2. Regions D1 and D2 are marked in Fig. 2a. The numbers on the top right of each panel are the spatial means for the area of the Gobi Desert, marked by the box in (a).

between DuEM and MERRA-2, the estimated percentage changes in dust emission over time are similar from both data sets. In the Gobi Desert, the negative trends are  $-7\%$  to  $-17\%$  decade $^{-1}$  and  $-10\%$  to  $-18\%$  decade $^{-1}$  (Fig. 7). The results are broadly consistent with the weakening in both the intensity and frequency of Mongolian cyclones over the years (Fig. 1c). The decrease in dust emissions associated with Mongolian cyclones is particularly notable in the northern Inner Mongolia Autonomous Region with more than  $-20\%$  decade $^{-1}$  (Fig. 7).

There is also a negative trend in  $\tau$  associated with atmospheric depressions and Mongolian cyclones, particularly in the region downwind of the Gobi Desert (black dashed box in Fig. 8a), which lies in the transport direction of dust-laden air by the cyclones. The decrease of  $\tau$  associated with Mongolian cyclones in that region is  $-11\%$  to  $-15\%$  decade $^{-1}$  (Fig. 8g, h),

consistent with the reported weakening of springtime dust storm frequency in previous studies<sup>8,47</sup>. Mongolian cyclones favor dust emissions in the Gobi Desert and the downward transport of dust aerosols, leading to relatively high regional mean  $\tau$  in the downwind region (compare the numbers in the top right of Fig. 5a–f to those in 5g–h). Hence, the decreasing intensity and frequency of Mongolian cyclones caused a decrease in mean dust emissions from the Gobi Desert, and therefore less downwind transport of dust aerosols.

### Mongolian cyclones and exceptional dust storms against their downward trend

While a decrease in dust emissions in the Gobi Desert and  $\tau$  in the downwind region is observed, individually strong dust storms nevertheless occur

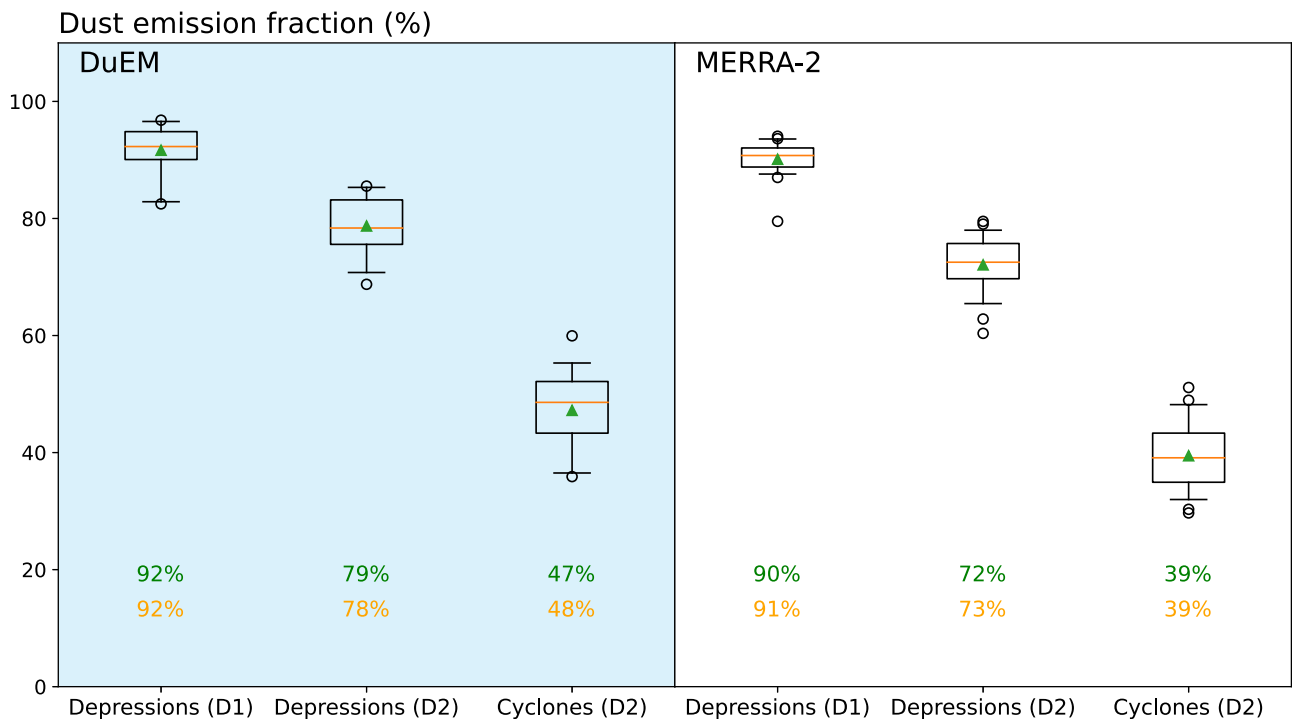


**Fig. 4 | Mean contributions of atmospheric depressions and Mongolian cyclones to springtime dust emissions in the Gobi Desert.** Shown are the distributions of the spatial mean fraction of dust emission in the Gobi Desert (black box in Fig. 3a) associated with atmospheric depressions and Mongolian cyclones for the detection

areas D1 and D2 (Fig. 2a). Mean fractions are marked by green triangles and green numbers at the bottom, medians are orange horizontal lines and orange numbers at the bottom, gray boxes are the 25–75% percentiles, whiskers are the 5–95% percentiles and circles are the outliers.

throughout the time series. We systematically assess the statistics in light of reported events in the literature to illustrate the role of Mongolian cyclones for high-impact East Asian dust storms, despite the mean decrease in their occurrence. The analysis includes the spring dust storm frequency in China obtained from the China Meteorological Administration (CMA) and the individual high-impact dust storms reported in previously peer-reviewed literature<sup>12,14–32</sup> where time and meteorological drivers of dust storms are given, marked in Fig. 9a. Moreover, we verified the occurrence of a visible cloud band and suspended dust aerosols as typical for cyclones (not shown) by visual inspection of the true color satellite images of the Moderate Resolution Imaging Spectroradiometer (MODIS) Aqua and Terra<sup>68</sup> and saw the characteristic features in most cases. All the reported individual dust storms included in our data are co-occurrence with the occurrence of Mongolian cyclones, except for the atmospheric depressions in 2010. We compute the maximum peak winds of these reported cyclones, when their center passes region D2 and mark them in Fig. 9a.

Since 2010, fewer dust storms have been observed over China (Fig. 9a), which aligns with the weakening in the peak winds and occurrence frequency of Mongolian cyclones and the associated dust emissions in the Gobi Desert and  $\tau$  in the region downwind (Figs. 1c, 7i, j and 8i, j). Moreover, more frequent Mongolian cyclone-driven dust emissions occur in Southern Mongolia than in Northern China as seen in the MERRA-2 analysis after 2017 (Fig. 9c). Hövmöller plots for the normalized monthly mean dust emission flux anomalies associated with Mongolian cyclones in D2 highlight that spatial evolution of the dust emissions (Fig. 9b, c). The northward movement of dust emissions over the years agrees with the faster decrease of dust emissions in Northern China than in Mongolia attributed to Mongolian cyclones (compare Fig. 9c to 7). Indeed, the mean position of Mongolian cyclone centers has shifted northward over the years (Fig. 9d), which is consistent with the reported poleward shift of the East Asian subtropical jet stream over the past decades<sup>69</sup>, and may contribute to the stronger decrease of dust emissions in Northern China and decrease of subsequent transport of dust aerosols. Moreover, the desertification in Southern Mongolia since 2010<sup>70</sup> may lead to a weaker decrease in dust activity in that region.

Dust emissions are also influenced by other factors such as dry soil and sparse vegetation<sup>8,47</sup>. For instance, conditions like high surface temperature, low precipitation, and excessive snow melt before the super dust storm in mid-March 2021 favor dust emissions<sup>50,51</sup>. The development of a Mongolian cyclone causes the necessary dust-emitting winds which leads to strong dust storms. This is supported by the high maximum peak winds in Mongolian cyclones during those previously reported individual dust storms from peer-reviewed publications (Fig. 9a), which are at least  $3 \text{ ms}^{-1}$  higher than dust emission threshold wind speed in the Gobi Desert ( $9.8 \pm 2.2 \text{ ms}^{-1}$ )<sup>34</sup>. Despite the mean weakening of the dust storm frequency and Mongolian cyclones, the occurrence of individual strong Mongolian cyclones can therefore still result in exceptionally severe dust storms as seen in the past few years. For example, four Mongolian cyclone-driven spring dust storms are observed in 2021, leading to slightly higher dust emissions in the Gobi Desert and  $\tau$  in East Asia (compare Figs. 7j, 8i, j and 9a).

## Discussion

As a main prerequisite for strong dust-emitting winds in the Gobi Desert, Mongolian cyclones have been investigated for previous super dust storms<sup>30,32</sup>. However, there have been no quantitative assessments on the relative contributions of atmospheric depressions and Mongolian cyclones to dust emission amounts and dust aerosol optical depth ( $\tau$ ) in East Asia from a climatological perspective. This study uses six datasets and extra-tropical cyclone tracks to address this knowledge gap.

Atmospheric depressions dominate the dust activity in East Asia, i.e., they explain ~90–92% of dust emissions in the Gobi Desert and ~88–93% of  $\tau$  in the downwind region, with differences depending on the data set. Similar contributions of atmospheric depressions to dust activities are found in other dust source regions, e.g., up to 90% of dust emissions in North Africa co-occur with atmospheric depressions<sup>46</sup>.

Mongolian cyclones are defined as long-living mobile atmospheric depressions, that form downstream of the Altai-Sayan Mountains. Mongolian cyclones support high-impact dust storms and explain almost half (~39–47%) of Gobi's dust emissions and ~34–43% of the  $\tau$  in the region

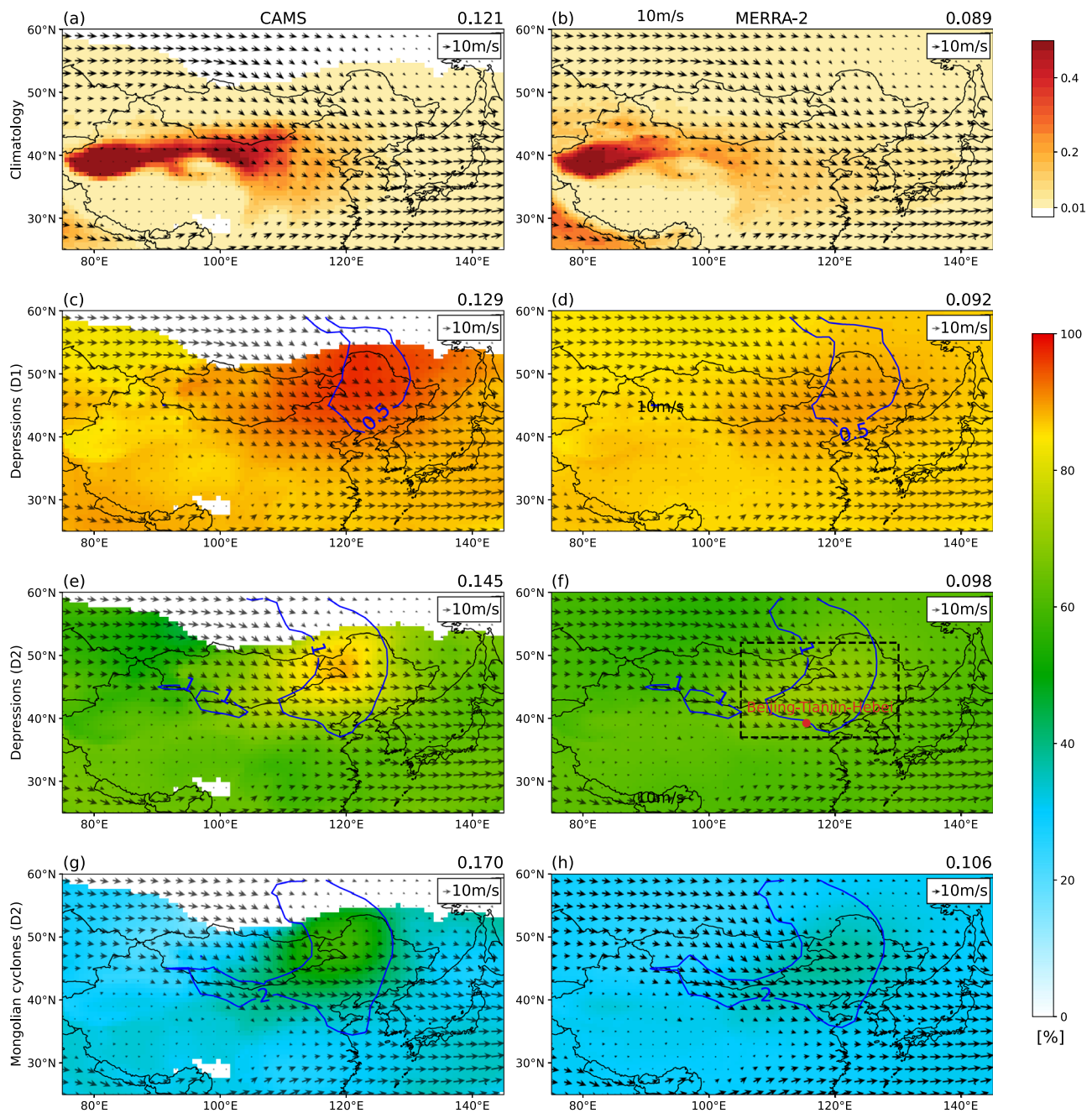


**Fig. 5 | Spatial pattern of the contributions of Mongolian cyclones to springtime dust aerosol optical depth ( $\tau$ ) for 2001–2022.** Shown are the mean  $\tau$  (shading) and 700 hPa wind vectors (arrows) for March to May from (a) CAMS and (b) MERRA-2 reanalysis, (c, d) like (a, b) but for the fraction of  $\tau$  and wind vectors at 700 hPa associated with atmospheric depressions detected in D1, (e, f) like (c, d) but for atmospheric depressions in D2, (g, h) like (e, f) but for Mongolian cyclones in D2.

Regions D1 and D2 are marked in Fig. 2a. The numbers on the top right are the composited mean  $\tau$  in Northeast China and East Mongolia as marked by black dashed box in (f). The blue contours in (c–h) indicate regions with anomalously high wind speeds at 700 hPa relative to the climatological mean. The red dot in (f) indicates the location of Beijing-Tianjin-Hebei region.

downwind in spring. The passage of Mongolian cyclones induces strong dust-emitting winds in the Gobi Desert, leading to high  $\tau$  and explain 19 of 20 high-impact dust storms from peer-reviewed publications. Cyclones in East Asia explain more regional dust emissions than in other deserts. For instance, in North Africa, only half as much (25%) of the dust emissions are induced by the passage of mobile cyclones<sup>46</sup>. At least in parts, this is due to more cyclogenesis over the Mongolian Plateau compared to the lee of the Atlas Mountains in North Africa.

Our study illustrates the consistent decrease in the occurrence frequency and intensity of Mongolian cyclones along with the associated dust emissions and  $\tau$  over the past 22 years. It suggests a direct

link of the decreasing Mongolian cyclones to the decrease of mean dust emissions and  $\tau$ . Previous studies indicate that the weakening of dust emission and dust storm frequency in Northern China is attributed to the decrease in mean near-surface winds<sup>8,47</sup>. In the present study, the dust-emitting winds in the Gobi Desert are positively correlated with the peak winds of Mongolian cyclones. Mongolian cyclones are a prerequisite for strong dust-emitting wind speeds in the Gobi Desert. Past studies suggest that reduced sea ice cover in the Barents Sea leads to a southward shift of the Rossby wave train over west Siberia and north China, affecting cyclogenesis over Mongolia<sup>71</sup>. In addition, Mongolian cyclones are also affected by the barotropic anomalous anticyclone over

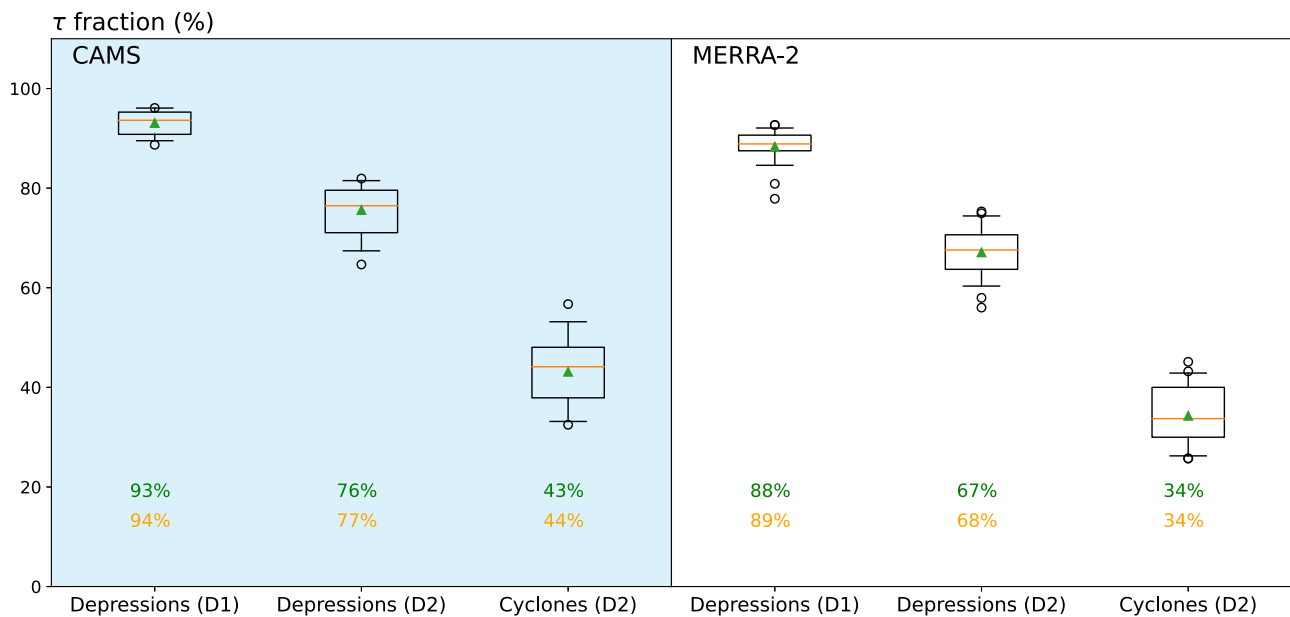


**Fig. 6 | Mean contributions of atmospheric depressions and Mongolian cyclones to spring  $\tau$ .** Shown are the distributions of the spatial mean fraction of  $\tau$  in the region of Northeast China and East Mongolia marked by the black dashed box in Fig. 5f associated with atmospheric depressions and Mongolian cyclones. Mean fractions

are represented as green triangles and green numbers at the bottom, medians are orange horizontal lines and orange numbers at the bottom, gray boxes represent the 25–75% percentiles, whiskers show the 5–95% percentiles, and circles are the outliers.

Northeast Asia induced by eastward-propagating upper-level waves train over the Eurasian continent associated with positive sea surface temperature (SST) anomalies in the North Atlantic<sup>72</sup>. Furthermore, the decrease in the intensity and frequency of Mongolian cyclones have been reported to be attributed to the weakened westerly jet stream and atmospheric baroclinicity due to the anthropogenic warming in northern China and Mongolian regions<sup>45</sup>.

However, strong individual Mongolian cyclones paired with exceptional dust storms occur against the mean declining trend. The results reveal that the mechanisms involved in the individually strong dust storms that are dominated by Mongolian cyclones should be investigated in more detail, particularly in the future when a decrease in the frequency of Mongolian cyclones is expected in the consistently warming world<sup>73</sup>. Furthermore, a previous case study analysis<sup>32</sup> suggests that the passage of Mongolian cyclones may also influence dust emissions in the Taklamakan Desert. Figure 3 suggests that Mongolian cyclones in D2 contribute ~34–39% of dust emission in the Taklamakan Desert. Detailed examinations of the dust emission mechanisms linked to the passage of Mongolian cyclones are necessary to establish a comprehensive understanding of the relative contributions of Mongolian cyclones to dust activities in the Taklamakan Desert in a continuously warming world.

## Methods

### Mongolian cyclone identification

The present study utilizes SLP, and wind speeds at 10 m a.g.l. from ERA5 reanalysis<sup>56</sup> for characterizing the occurrence frequency and intensity of Mongolian cyclones<sup>54,55</sup>. As the fifth generation of the ECMWF reanalysis, ERA5 integrates a modern weather model with observations, creating a temporally and spatially consistent dataset with a temporal resolution of 1 h and horizontal resolution of 0.25°<sup>56</sup>. ERA5 is used to characterize meteorological conditions for Mongolian cyclones-related dust storms and shows skill in representing meteorological variables, such as temperature at 2 m a.g.l., and wind speed at 10 m a.g.l.<sup>32</sup>.

The Mongolian cyclones are selected from the dataset of atmospheric depressions, which are automatically identified with a detection algorithm<sup>54,55</sup> applied to ERA5 reanalysis data<sup>56</sup>. The atmospheric depressions are

identified as the finite area surrounding the center. The center of an atmospheric depression is the grid point where the SLP is more than 2 hPa lower than that of its eight surrounding points. After detecting the center of an atmospheric depression, a tracking algorithm is used to combine the centers across time into one coherent system to determine the track. At time  $t_{n+1}$ , an atmospheric depression center  $x_p(t_{n+1})$  is combined with the previous one  $x_Q(t_n)$ , when the distance between  $x_p(t_{n+1})$  and a guess location of  $x_Q(t_{n+1})$  is less than 1000 km. The guess location is estimated with the equation of  $x_Q(t_{n+1}) = x_Q(t_n) + 0.75[x_Q(t_n) - x_Q(t_{n-1})]$ . The genesis is the first grid point of the track, i.e., technically when no previous displacement vector is available to estimate the guess location. Lysis is the last grid point of a track, i.e., when no atmospheric depression center is found for the subsequent time. Finally, all identified tracks are labeled with an index, and the lifetime of each atmospheric depression is computed as the time difference between genesis and lysis<sup>54,55</sup>.

For the automated detection of atmospheric depressions, the SLP data from ERA5 reanalysis with a temporal resolution of 1 h was used. The identified depressions can be stationary or mobile, and include for instance the frequently detected heat lows over the Taklamakan Desert (not shown). The tracking algorithm combines several individually identified depressions into temporal sequences of identification of the same system. To separate the mobile extra-tropical cyclones forming over Mongolia, we select the tracks in spring and filter the resulting data with the following criteria:

1. The cyclones have to have a lifetime of at least 24 h, consistent with previous studies on extra-tropical cyclones in East Asia<sup>74,75</sup>.
2. The cyclones have to be mobile and travel a distance of more than 5° in longitude, similar to an earlier work of extra-tropical cyclones in East Asia<sup>75</sup>.
3. Mongolian cyclones have to be generated downstream of the Altai-Sayan Mountain, i.e., the genesis of the mobile cyclone track occurs specifically in the region of 90°E–120°E and 40°N–53°N (marked in Fig. 1a) similar to previous studies<sup>44,76</sup>. Specifically, the pressure ridge (trough) is seen in the luv (lee) of the Altai-Sayan Mountains in the mid-troposphere and the genesis of a Mongolian cyclone is seen as a negative pressure anomaly at low tropospheric levels in the lee of the mountains<sup>60</sup>.



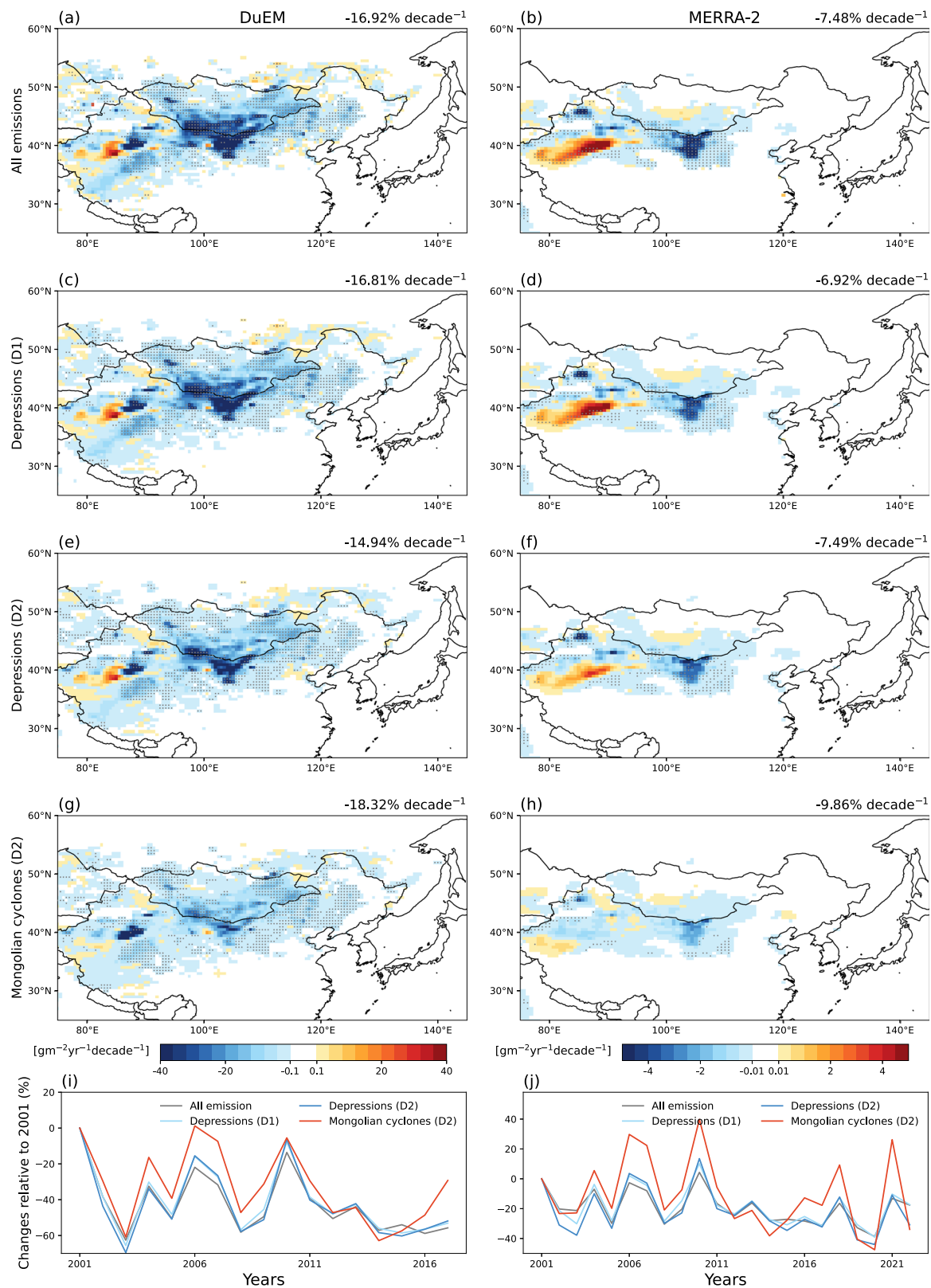


**Fig. 7 | Trends in dust emissions associated with atmospheric depressions and Mongolian cyclones.** Shown are linear trends in springtime dust emission fluxes for 2001–2022 from (a) DuEM and (b) MERRA-2 reanalysis, (c, d) like (a, b) but for spring dust emissions co-occurring with atmospheric depressions in D1, (e, f) like (c, d) but with atmospheric depressions in D2, (g, h) like (c, d) but with Mongolian cyclones in D2, and (i, j) changes in regional mean spring dust emissions in the Gobi

Desert associated with atmospheric depressions and Mongolian cyclones, relative to 2001. Black dots in (a–h) indicate where the trends are significant at the 90% confidence level. The numbers on the top right of (a–h) are the spatially averaged trends in spring dust emission for the Gobi Desert, marked in Fig. 3a. D1 and D2 are marked in Fig. 2a.

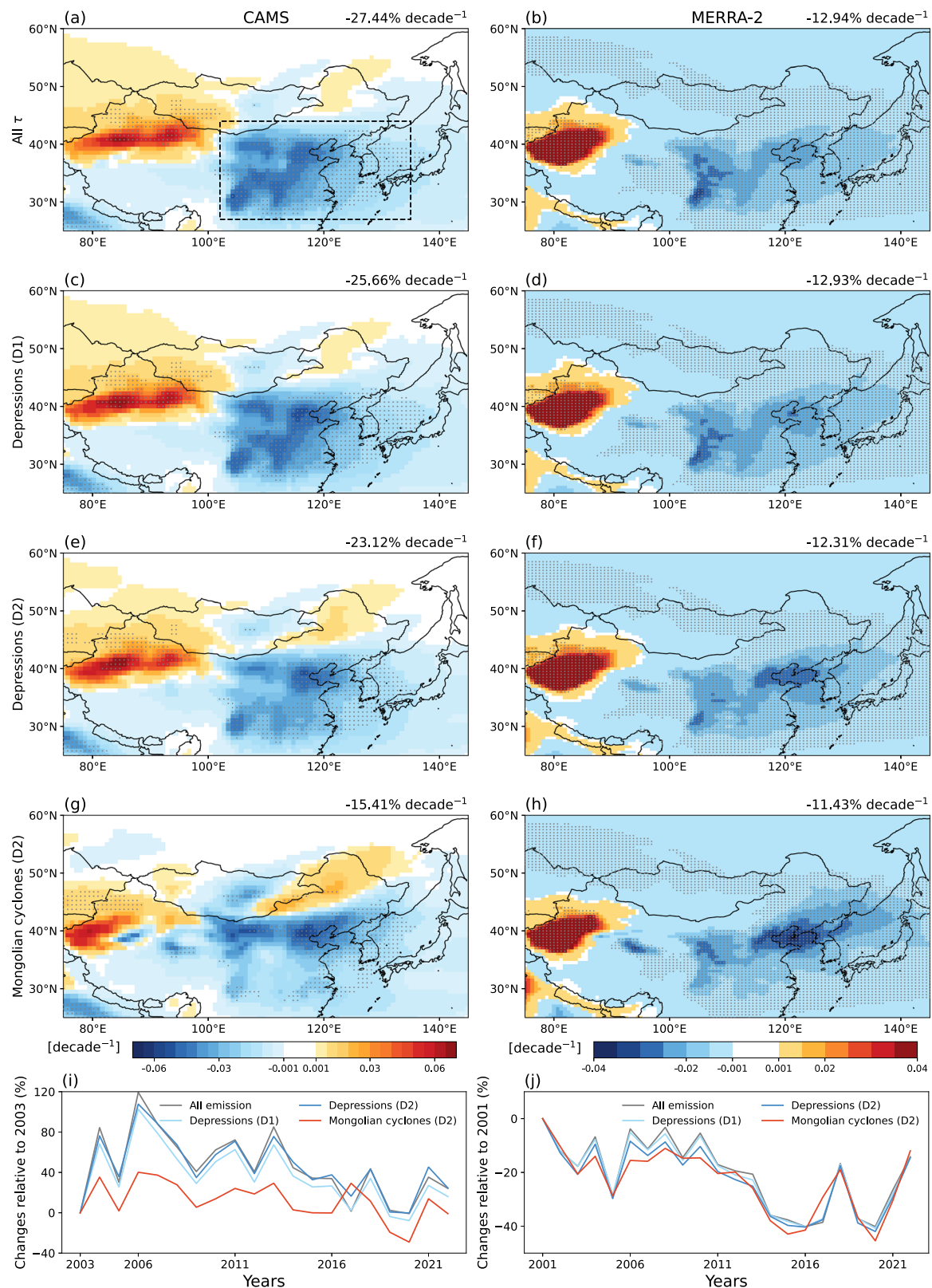


**Fig. 8 | Trends in  $\tau$  associated with atmospheric depressions and Mongolian cyclones.** Shown are linear trends in springtime  $\tau$  for 2001–2022 from (a) CAMS and (b) MERRA-2 reanalysis, (c, d) like (a, b) but for spring  $\tau$  co-occurring with atmospheric depressions in D1, (e, f) like (c, d) but with atmospheric depressions in D2, (g, h) like (c, d) but with Mongolian cyclones in D2, and (i, j) changes in regional mean spring  $\tau$  in the region marked as black dashed box in (a) associated with

atmospheric depressions and Mongolian cyclones, relative to 2003 (CAMS) and 2001 (MERRA-2) respectively. Black dots in (a–h) indicate where the trends are significant at the 90% confidence level. The numbers on the top right of (a–h) are the spatially averaged trends in spring  $\tau$  for the black dashed box in (a). D1 and D2 are marked in Fig. 2a.

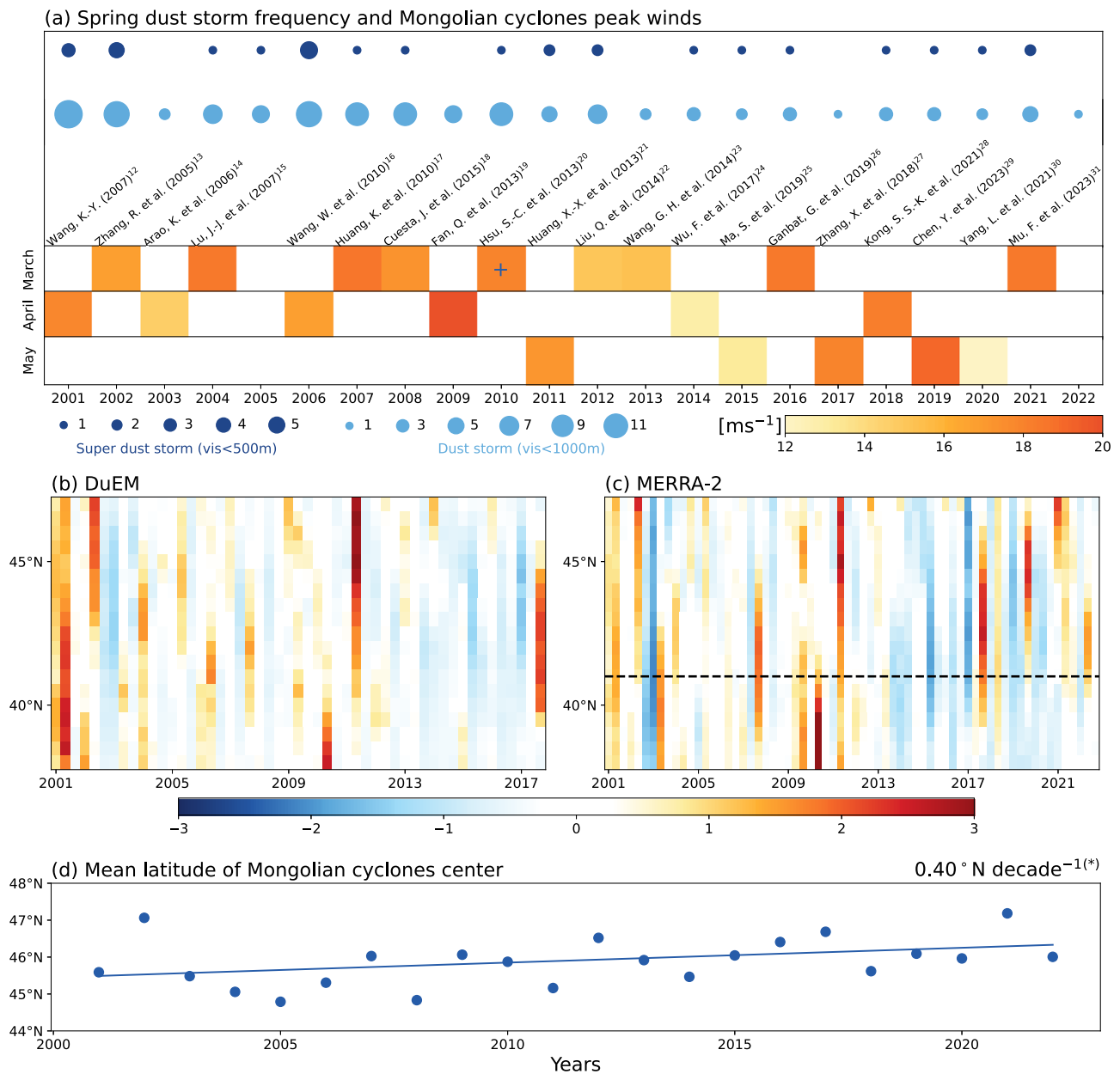


**Fig. 9 | Co-occurrence of Mongolian cyclones and East Asian dust storms in springtime.** Show are (a) the number of spring super dust storms and dust storms (including super dust storms) over China and the maximum peak winds of the associated Mongolian cyclone in D2 during individual dust storms as reported by peer-reviewed publications from 2001 to 2022, (b, c) Hovmöller plot of monthly mean dust emission flux anomalies, normalized by the climatological standard deviation, associated with Mongolian cyclones in D2 from DuEM (2001–2017) and MERRA-2 (2001–2022) reanalysis, and (d) mean position (latitude) of Mongolian cyclones center detected in D2 per spring and their trends from 2001 to 2022. The

occurrences of dust storms are obtained from the China Meteorological Administration measured by in-situ observations of atmospheric visibility across China and validated against past studies addressing the dust storm dynamics. Region D2 is marked as a red box in Fig. 2a. The dust storm event in 2010 is associated with the defined atmospheric depressions with a lifetime of less than 24 h, marked with +. The black dashed line in (c) represents the latitude at 104.5°E and 41°N, located in northern China near the border with Mongolia. (\*) in (d) indicates that the statistical significance exceeds the 90% confidence level.

### Dust data

To investigate the contributions of Mongolian cyclones to East Asian springtime dust activity, we obtain data from multiple sources, including dust storm occurrence, MODIS true color images, dust emission flux, and dust aerosol optical depth ( $\tau$ ), as follows.

Reports of spring dust storms in China are taken from the CMA for 2001–2022. CMA publishes yearly China Climate Bulletins which include extreme meteorological disasters, e.g., rainstorms, dust storms, severe convection, and floods. The classification of dust events is based on the in-situ observations of atmospheric visibility at weather stations in China<sup>43,77</sup>.

Dust storms are defined as weather conditions when the visibility is less than 1000 m, and super dust storms are less than 500 m.

Data for the dust emission flux are obtained from DuEM<sup>47</sup>, and MERRA-2 reanalysis<sup>57</sup>. DuEM uses the Shao04 dust emission parameterization scheme<sup>65</sup>, where vertical dust emission fluxes are calculated with the main mechanism of saltation bombardment and aggregate disintegration over surfaces with barren land, grasslands, and croplands in northeastern China. Dust emission flux in DuEM is simulated in 4 size bins, namely 0–2.5  $\mu\text{m}$ , 2.5–5  $\mu\text{m}$ , 5–10  $\mu\text{m}$ , and 10–20  $\mu\text{m}$ . MERRA-2 global atmospheric reanalysis for the satellite era is generated by the National

Aeronautics and Space Administration (NASA) Global Modeling and Assimilation Office with the Goddard Earth Observing System Model<sup>78</sup>. Dust aerosols in MERRA-2 are calculated with the Global Ozone Chemistry Aerosol Radiation and Transport model, where barren land surfaces are potential dust sources<sup>66</sup>. Dust aerosols are simulated in 5 size bins in MERRA-2, namely 0.2–2  $\mu\text{m}$ , 2–3.6  $\mu\text{m}$ , 3.6–6  $\mu\text{m}$ , 6–12  $\mu\text{m}$ , and 12–20  $\mu\text{m}$ , and are provided as time-averaged data. Given the uncertainty in dust simulations<sup>79–82</sup>, we have chosen to include two different estimates of dust emission fluxes that include observational data to constrain the simulation. We utilize dust emission flux data from DuEM in spring from 2001–2017 with a temporal resolution of 1 h and a horizontal resolution of  $0.5^\circ \times 0.625^\circ$ <sup>47</sup>. Furthermore, we use dust emission fluxes<sup>57</sup> and  $\tau$  at 550 nm<sup>58</sup> from MERRA-2 reanalysis for March to May in the years 2001–2022. The temporal resolution of the MERRA-2 output is 1 h with a horizontal resolution  $0.5^\circ \times 0.625^\circ$ .

In addition to  $\tau$  from MERRA-2, we use data from the reanalysis of the CAMS, specifically the fourth generation of ECMWF's Atmospheric Composition Reanalysis 4<sup>59</sup>. The global atmospheric composition data is available since 2003 and has been created by assimilating observational data into ECMWF's Integrated Forecast System. Dust aerosols in CAMS reanalysis are represented in 3 size bins, namely 0.06–1.1  $\mu\text{m}$ , 1.1–1.8  $\mu\text{m}$ , and 1.8–40  $\mu\text{m}$ , and are provided as instantaneous data. Here, the  $\tau$  at 550 nm from CAMS reanalysis for the spring months in 2003–2022 is used. The CAMS data in this study has a temporal resolution of 3 h and a horizontal resolution of  $0.75^\circ$ .

### Analysis strategy

To better understand the spatial pattern of Mongolian cyclones, the present study computes the cyclogenesis and occurrence frequency of Mongolian cyclones within a cyclone-affected area. The cyclone-affected area is defined as the region within a  $5^\circ$  radius around each center of Mongolian cyclones, following the approach of a previous East Asian extratropical cyclone climatology<sup>44</sup>. Cyclogenesis in Fig. 1a refers to the cyclone-affected area during the genesis of the detected cyclones. Occurrence frequency (Fig. 1b) is defined as the number of occurrences of cyclone-affected areas at each grid box. The same event is only counted once for the calculation of occurrence frequency. To measure the cyclone intensity, we compute the horizontally averaged maximum in 10 m wind speeds that occur in the cyclone-affected area and refer to it as peak winds of Mongolian cyclones. Similarly, a comparable size of the cyclone-affected area and the definition of cyclone intensity have been used for an earlier study<sup>83</sup>. We further analyse the linear trends of the number of Mongolian cyclones and mean peak winds in each spring and the statistical distributions of lifetime, travel distance in geographical longitude, mean peak winds, and maximum peak winds of Mongolian cyclones and all identified East Asian atmospheric depressions (Fig. 1c–g).

To identify the region where Mongolian cyclones often lead to extreme dust emissions in the Gobi Desert ( $97^\circ\text{E}$ – $112^\circ\text{E}$  and  $38^\circ\text{N}$ – $46^\circ\text{N}$ ), we computed composited anomalies of SLP when the spatially averaged hourly dust emission flux exceeds the 95th percentile in this desert, with data from DuEM and MERRA-2. Both results show a relatively lower composite-mean SLP over southeastern Mongolia and Northern China (Fig. 2a, b), even though the magnitudes of the simulated dust emission fluxes differ between DuEM and MERRA-2. A similar region with an identified low-pressure system that is associated with spring dust storms is also found in a previous study<sup>43</sup>. A scatter plot of daily maximum wind speeds at 10 m a.g.l. across the Gobi Desert and the daily maximum peak wind speeds of Mongolian cyclones passing D2 is used to illustrate the effects of Mongolian cyclones on dust-emitting wind speeds in the Gobi Desert (Fig. 2c). We, therefore, choose region D2 (red box in Fig. 2a) for the analysis of the occurrence of Mongolian cyclones and dust activities in springtime from 2001 to 2022. In addition to D2, a relatively larger region (D1, black box in Fig. 2a) is also selected to include more dust emissions associated with atmospheric depressions.

When the centers, identified from the automated detection algorithm, of Mongolian cyclones (atmospheric depressions) are in D2 (D1 and D2),

we compute the contributions of Mongolian cyclones (atmospheric depressions) to the springtime dust storm activity as an averaged fraction of the annual total emission amount for spring months in the period 2001–2022. Specifically, we compute the ratio of dust emissions and  $\tau$  associated with Mongolian cyclones and atmospheric depressions to the total dust emissions and  $\tau$  in spring (Figs. 3, 4, 5, and 6). Since dust aerosols generated from the Gobi Desert are typically transported between 2 and 4 km a.g.l.<sup>40</sup>, we show the wind vectors at 700 hPa from ERA5 reanalysis in Fig. 5 to illustrate the effects of atmospheric depressions and Mongolian cyclones on dust aerosol transport. We also show the linear trends of springtime dust emissions and  $\tau$  associated with atmospheric depressions and Mongolian cyclones for 2001–2022 (Figs. 7 and 8). The percentage changes for the spatially averaged trends in the top right of Figs. 7 and 8 are calculated relative to total annual dust emission flux and the mean  $\tau$  of 2001 (DuEM and MERRA-2) and 2003 (CAMS).

Additionally, we analyze recorded events of super dust storms and the peak winds of Mongolian cyclones to illustrate the occurrence of severe dust storms due to Mongolian cyclones as perceived from published case studies, despite the negative trend in cyclone number (Fig. 9). We calculate the maximum peak winds during the automatically detected Mongolian cyclones, and in the case of 2010 for the atmospheric depression, in D2, based on the recorded individual dust storms from peer-reviewed publications. The spring mean of the latitude of all Mongolian cyclone centers and the associated trends for 2001–2022 is shown in Fig. 9d. We compute the latitude-dependent anomalies in the mean dust emission fluxes for spring months against their mean monthly climatology associated with Mongolian cyclones and normalize the anomalies by the standard deviation in the monthly fluxes to assess the spatio-temporal changes of dust storms (Fig. 9b, c).

### Data availability

ERA5 reanalysis is available at the ECMWF Copernicus Climate Data Store (<https://cds.climate.copernicus.eu/>). The CAMS reanalysis data is available at the ECMWF Copernicus Atmosphere Data Store (<https://ads.atmosphere.copernicus.eu/>). MERRA-2 reanalysis is available at the Global Modeling and Assimilation Office of National Aeronautics and Space Administration ([https://gmao.gsfc.nasa.gov/reanalysis/MERRA-2/data/\\_access/](https://gmao.gsfc.nasa.gov/reanalysis/MERRA-2/data/_access/)). Dust emissions from DuEM are available at the Science Data Bank (<https://doi.org/10.57760/sciencedb.03301>). Dust storm reports are available from the China Meteorological Administration (CMA; <http://www.cma.gov.cn/en/>) and MODIS images for dust storms and Mongolian cyclones are available at the NASA Worldview (<https://worldview.earthdata.nasa.gov/>).

Received: 28 August 2024; Accepted: 24 January 2025;

Published online: 15 February 2025

### References

- De Longueville, F., Hountondji, Y.-C., Henry, S. & Ozer, P. What do we know about effects of desert dust on air quality and human health in West Africa compared to other regions? *Sci. Total Environ.* **409**, 1–8 (2010).
- Kok, J. F., Ward, D. S., Mahowald, N. M. & Evan, A. T. Global and regional importance of the direct dust-climate feedback. *Nat. Commun.* **9**, 241 (2018).
- Schweitzer, M. D. et al. Lung health in era of climate change and dust storms. *Environ. Res.* **163**, 36–42 (2018).
- Kok, J. F. et al. Contribution of the world's main dust source regions to the global cycle of desert dust. *Atmos. Chem. Phys.* **21**, 8169–8193 (2021).
- Huang, J., Wang, T., Wang, W., Li, Z. & Yan, H. Climate effects of dust aerosols over East Asian arid and semiarid regions. *J. Geophys. Res. Atmos.* **119**, 11,398–11,416 (2014).
- Shao, Y. & Dong, C. A review on East Asian dust storm climate, modelling and monitoring. *Glob. Planet. Chang.* **52**, 1–22 (2006).



7. Chen, S. et al. Regional modeling of dust mass balance and radiative forcing over East Asia using WRF-Chem. *Aeolian Res.* **15**, 15–30 (2014).
8. Yao, W., Gui, K., Wang, Y., Che, H. & Zhang, X. Identifying the dominant local factors of 2000–2019 changes in dust loading over East Asia. *Sci. Total Environ.* **777**, 146064 (2021).
9. Huang, J. et al. Possible influences of Asian dust aerosols on cloud properties and radiative forcing observed from MODIS and CERES. *Geophys. Res. Lett.* **33**, L06824 (2006).
10. Wang, Y. et al. Effects of dust storm events on weekly clinic visits related to pulmonary tuberculosis disease in Minqin, China. *Atmos. Environ.* **127**, 205–212 (2016).
11. Filonchik, M. & Peterson, M. Development, progression, and impact on urban air quality of the dust storm in Asia in March 15–18, 2021. *Urban Clim.* **41**, 101080 (2022).
12. Zhang, X. et al. East Asian dust storm in May 2017: observations, modelling, and its influence on the Asia-Pacific region. *Atmos. Chem. Phys.* **18**, 8353–8371 (2018).
13. Wang, W. & Zhang, J. The population affected by dust in China in the springtime. *Plos one* **19**, e0281311 (2024).
14. Wang, K.-Y. Long-range transport of the April 2001 dust clouds over the subtropical East Asia and the North Pacific and its impacts on ground-level air pollution: a Lagrangian simulation. *J. Geophys. Res. Atmos.* **112**, D09203 (2007).
15. Zhang, R., Arimoto, R., An, J., Yabuki, S. & Sun, J. Ground observations of a strong dust storm in Beijing in March 2002. *J. Geophys. Res. Atmos.* **110**, D18S06 (2005).
16. Arao, K. et al. Yellow sand dust event on 13 April 2003 over western Kyushu, Japan. *SOLA* **2**, 100–103 (2006).
17. Lu, J.-J., Zhao, L.-N. & Du, B.-Y. The real time numerical prediction and characteristics of a severe dust storm covers China in the spring of 2004. *Clim. Environ. Res.* **12**, 188–198 (2007).
18. Wang, W. et al. Insights into an Asian dust event sweeping Beijing during April 2006: Particle chemical composition, boundary layer structure, and radiative forcing. *J. Geophys. Res. Atmos.* **115**, D18208 (2010).
19. Huang, K. et al. Mixing of Asian dust with pollution aerosol and the transformation of aerosol components during the dust storm over China in spring 2007. *J. Geophys. Res. Atmos.* **115**, D00K13 (2010).
20. Cuesta, J. et al. Three-dimensional distribution of a major desert dust outbreak over East Asia in March 2008 derived from IASI satellite observations. *J. Geophys. Res. Atmos.* **120**, 7099–7127 (2015).
21. Fan, Q. et al. Impact of a dust storm on characteristics of particle matter (PM) in Guangzhou, China. *Asia Pac. J. Atmos. Sci.* **49**, 121–131 (2013).
22. Hsu, S.-C. et al. A super Asian dust storm over the East and South China seas: disproportionate dust deposition. *J. Geophys. Res. Atmos.* **118**, 7169–7181 (2013).
23. Huang, X.-X. et al. Studies on a severe dust storm in East Asia and its impact on the air quality of Nanjing, China. *Aerosol Air Qual. Res.* **13**, 179–193 (2013).
24. Liu, Q., Liu, Y., Yin, J., Zhang, M. & Zhang, T. Chemical characteristics and source apportionment of PM<sub>10</sub> during Asian dust storm and non-dust storm days in Beijing. *Atmos. Environ.* **91**, 85–94 (2014).
25. Wang, G. H. et al. Evolution of aerosol chemistry in Xi'an, inland China, during the dust storm period of 2013—part 1: sources, chemical forms and formation mechanisms of nitrate and sulfate. *Atmos. Chem. Phys.* **14**, 11571–11585 (2014).
26. Wu, F. et al. Limited production of sulfate and nitrate on front-associated dust storm particles moving from desert to distant populated areas in northwestern China. *Atmos. Chem. Phys.* **17**, 14473–14484 (2017).
27. Ma, S. et al. Multimodel simulations of a springtime dust storm over northeastern China: implications of an evaluation of four commonly used air quality models (CMAQ v5.2.1, CAMx v6.50, CHIMERE v2017r4, and WRF-Chem v3.9.1). *Geosci. Model Dev.* **12**, 4603–4625 (2019).
28. Ganbat, G. & Jugder, D. Observations and transport modeling of dust storm event over Northeast Asia using HYSPLIT: case study. In *E3S Web Conferences* Vol. 99, 02002 (EDP Sciences, 2019).
29. Kong, S. S.-K. et al. Sensitivity analysis of the dust emission treatment in CMAQv5.2.1 and its application to long-range transport over East Asia. *Atmos. Environ.* **257**, 118441 (2021).
30. Chen, Y. et al. A super dust storm enhanced by radiative feedback. *npj Clim. Atmos. Sci.* **6**, 90 (2023).
31. Yang, L. et al. Detection of a dust storm in 2020 by a multi-observation platform over the northwest China. *Remote Sens.* **13**, 1056 (2021).
32. Mu, F., Luiz, E. W. & Fiedler, S. On the dynamics and air-quality impact of the exceptional East Asian dust outbreak in mid-March 2021. *Atmos. Res.* **292**, 106846 (2023).
33. Kok, J. F. et al. Mineral dust aerosol impacts on global climate and climate change. *Nat. Rev. Earth Environ.* **4**, 71–86 (2023).
34. Kurosaki, Y. & Mikami, M. Threshold wind speed for dust emission in East Asia and its seasonal variations. *J. Geophys. Res. Atmos.* **112**, D17202 (2007).
35. Zhao, S. et al. Urban particle size distributions during two contrasting dust events originating from Taklimakan and Gobi Deserts. *Environ. Pollut.* **207**, 107–122 (2015).
36. Chen, S. et al. Emission, transport, and radiative effects of mineral dust from the Taklimakan and Gobi deserts: comparison of measurements and model results. *Atmos. Chem. Phys.* **17**, 2401–2421 (2017).
37. Ge, J. M., Liu, H., Huang, J. & Fu, Q. Taklimakan Desert nocturnal low-level jet: climatology and dust activity. *Atmos. Chem. Phys.* **16**, 7773–7783 (2016).
38. Yuan, T. et al. Influence of dynamic and thermal forcing on the meridional transport of Taklimakan Desert dust in spring and summer. *J. Clim.* **32**, 749–767 (2019).
39. Spengler, T. & Smith, R. K. The dynamics of heat lows over flat terrain. *Q. J. R. Meteorol. Soc.* **134**, 2157–2172 (2008).
40. Chen, S. et al. Comparison of dust emissions, transport, and deposition between the Taklimakan Desert and Gobi Desert from 2007 to 2011. *Sci. China Earth Sci.* **60**, 1338–1355 (2017).
41. Tao, M. et al. Characterization of dust activation and their prevailing transport over East Asia based on multi-satellite observations. *Atmos. Res.* **265**, 105886 (2022).
42. Takemi, T. & Seino, N. Dust storms and cyclone tracks over the arid regions in east Asia in spring. *J. Geophys. Res. Atmos.* **110**, D18S11 (2005).
43. Li, J. et al. Predominant type of dust storms that influences air quality over Northern China and future projections. *Earth's. Futur.* **10**, e2022EF002649 (2022).
44. Lee, J. et al. Extratropical cyclones over East Asia: climatology, seasonal cycle, and long-term trend. *Clim. Dyn.* **54**, 1131–1144 (2020).
45. Zhu, C., Wang, B. & Qian, W. Why do dust storms decrease in northern China concurrently with the recent global warming? *Geophys. Res. Lett.* **35**, L18702 (2008).
46. Fiedler, S., Schepanski, K., Knippertz, P., Heinold, B. & Tegen, I. How important are atmospheric depressions and mobile cyclones for emitting mineral dust aerosol in North Africa? *Atmos. Chem. Phys.* **14**, 8983–9000 (2014).
47. Wu, C., Lin, Z., Shao, Y., Liu, X. & Li, Y. Drivers of recent decline in dust activity over East Asia. *Nat. Commun.* **13**, 7105 (2022).
48. Zhang, G. et al. Uneven Warming likely contributed to declining near-surface wind speeds in northern China between 1961 and 2016. *J. Geophys. Res. Atmos.* **126**, e2020JD033637 (2021).
49. Liu, J. et al. Impact of Arctic amplification on declining spring dust events in East Asia. *Clim. Dyn.* **54**, 1913–1935 (2020).
50. Yin, Z., Wan, Y., Zhang, Y. & Wang, H. Why super sandstorm 2021 in North China? *Natl Sci. Rev.* **9**, nwab165 (2021).
51. Gui, K. et al. Record-breaking dust loading during two mega dust storm events over northern China in March 2021: aerosol optical and radiative properties and meteorological drivers. *Atmos. Chem. Phys.* **22**, 7905–7932 (2022).

52. Hu, Z. et al. Attribution of the March 2021 exceptional dust storm in North China. *Bull. Am. Meteorol. Soc.* **104**, E749 – E755 (2023).
53. Bueh, C., Zhuge, A., Xie, Z., Yong, M. & Purevjav, G. The development of a powerful Mongolian cyclone on 14–15 March 2021: Eddy energy analysis. *Atmos. Ocean. Sci. Lett.* **15**, 100259 (2022).
54. Wernli, H. & Schwierz, C. Surface cyclones in the ERA-40 dataset (1958–2001). part I: Novel identification method and global climatology. *J. Atmos. Sci.* **63**, 2486 – 2507 (2006).
55. Sprenger, M. et al. Global climatologies of Eulerian and Lagrangian flow features based on era-interim. *Bull. Am. Meteorol. Soc.* **98**, 1739 – 1748 (2017).
56. Hersbach, H. et al. The ERA5 global reanalysis. *Q. J. Roy. Meteor. Soc.* **146**, 1999–2049 (2020).
57. GMAO. MERRA-2 tavg1\_2d\_adg\_Nx: 2d,1-Hourly, Time-averaged, Single-Level, Assimilation, Aerosol Diagnostics (extended) V5.12.4, Greenbelt, MD, USA, Goddard Earth Sciences Data and Information Services Center (GES DISC), accessed 1 June 2023 (2015).
58. GMAO. MERRA-2 tavg1\_2d\_adg\_Nx: 2d,1-Hourly, Time-averaged, Single-Level, Assimilation, Aerosol Diagnostics V5.12.4, Greenbelt, MD, USA, Goddard Earth Sciences Data and Information Services Center (GES DISC), accessed 1 June 2023 (2015).
59. Inness, A. et al. The CAMS reanalysis of atmospheric composition. *Atmos. Chem. Phys.* **19**, 3515–3556 (2019).
60. Chen, S.-J. & Lazić, L. Numerical case study of the Altai-Sayan lee cyclogenesis over east Asia. *Meteorol. Atmos. Phys.* **42**, 221–229 (1990).
61. Bleck, R. Numerical simulation of lee cyclogenesis in the Gulf of Genoa. *Mon. Weather Rev.* **105**, 428 – 445 (1977).
62. Mesinger, F., Janjić, Z. I., Ničković, S., Gavrilov, D. & Deaven, D. G. The step-mountain coordinate: model description and performance for cases of Alpine lee cyclogenesis and for a case of an Appalachian redevelopment. *Mon. Weather Rev.* **116**, 1493 – 1518 (1988).
63. He, Y. et al. Mega Asian dust event over China on 27–31 March 2021 observed with space-borne instruments and ground-based polarization lidar. *Atmos. Environ.* **285**, 119238 (2022).
64. Qian, W. et al. Anomaly based synoptic analysis and model prediction of six dust storms moving from Mongolia to Northern China in spring 2021. *J. Geophys. Res. Atmos.* **127**, e2021JD036272 (2022).
65. Shao, Y. Simplification of a dust emission scheme and comparison with data. *J. Geophys. Res. Atmos.* **109**, D10202 (2004).
66. Ginoux, P. et al. Sources and distributions of dust aerosols simulated with the GOCART model. *J. Geophys. Res. Atmos.* **106**, 20255–20273 (2001).
67. Chen, B. et al. Analysis of long-term trends in the vertical distribution and transport paths of atmospheric aerosols in typical regions of China using 15 years of CALIOP Data. *J. Geophys. Res. Atmos.* **128**, e2022JD038066 (2023).
68. Kaufman, Y. J., Tanré, D. & Boucher, O. A satellite view of aerosols in the climate system. *Nature* **419**, 215–223 (2002).
69. Yin, J. & Zhang, Y. Decadal changes of East Asian jet streams and their relationship with the mid-high latitude circulations. *Clim. Dyn.* **56**, 2801–2821 (2021).
70. Xu, S., Wang, J., Altansukh, O. & Chuluun, T. Spatiotemporal evolution and driving mechanisms of desertification on the Mongolian Plateau. *Sci. Total Environ.* **941**, 173566 (2024).
71. Fan, K., Xie, Z., Wang, H., Xu, Z. & Liu, J. Frequency of spring dust weather in North China linked to sea ice variability in the Barents Sea. *Clim. Dyn.* **51**, 4439–4450 (2018).
72. Liu, B. & Zhu, C. Extremely late onset of the 2018 South China Sea summer monsoon following a la niña event: effects of triple sst anomaly mode in the North Atlantic and a weaker Mongolian cyclone. *Geophys. Res. Lett.* **46**, 2956–2963 (2019).
73. Lee, J., Hwang, J., Son, S.-W. & Gyakum, J. R. Future changes of East Asian extratropical cyclones in the cmip5 models. *J. Clim.* **35**, 6911 – 6921 (2022).
74. Wang, X., Zhai, P. & Wang, C. Variations in extratropical cyclone activity in northern East Asia. *Adv. Atmos. Sci.* **26**, 471–479 (2009).
75. Zhang, Y., Ding, Y. & Li, Q. A climatology of extratropical cyclones over East Asia during 1958–2001. *Acta Oceanol. Sin.* **26**, 261 – 277 (2012).
76. Wang, J., Chen, L. & Li, S. Characteristics of spring Mongolian cyclones in the recent 70 years: background circulations and weather influences. *Int. J. Climatol.* **44**, 328–343 (2024).
77. Zhang, X. et al. Mapping the seamless hourly surface visibility in China: a real-time retrieval framework using a machine-learning-based stacked ensemble model. *npj Clim. Atmos. Sci.* **7**, 68 (2024).
78. Molod, A., Takacs, L., Suarez, M. & Bacmeister, J. Development of the GEOS-5 atmospheric general circulation model: evolution from MERRA to MERRA2. *Geosci. Model Dev.* **8**, 1339–1356 (2015).
79. Lee, J.-H. & Lee, S.-H. Modeling a severe wintertime Asian dust event observed in the East Asia region: sensitivity of the WRF-Chem dust emission schemes. *Atmos. Pollut. Res.* **13**, 101599 (2022).
80. Wu, C., Lin, Z. & Liu, X. The global dust cycle and uncertainty in cmip5 (coupled model intercomparison project phase 5) models. *Atmos. Chem. Phys.* **20**, 10401–10425 (2020).
81. Zhao, J., Ma, X., Wu, S. & Sha, T. Dust emission and transport in Northwest China: WRF-Chem simulation and comparisons with multi-sensor observations. *Atmos. Res.* **241**, 104978 (2020).
82. Zhao, A., Ryder, C. L. & Wilcox, L. J. How well do the cmip6 models simulate dust aerosols? *Atmos. Chem. Phys.* **22**, 2095–2119 (2022).
83. Pfahl, S. & Sprenger, M. On the relationship between extratropical cyclone precipitation and intensity. *Geophys. Res. Lett.* **43**, 1752–1758 (2016).

## Acknowledgements

We thank Michael Sprenger and Heini Wernli from ETH Zürich for providing the atmospheric depressions data and Michael Sprenger for commenting on an earlier version of the manuscript. Moreover, we thank the European Centre for Medium-Range Weather Forecasts for providing ERA5 and CAMS data, the Global Modeling and Assimilation Office of the National Aeronautics and Space Administration for MERRA-2 reanalysis, the China Meteorological Administration for the dust storm reports available, NASA Worldview for the MODIS true color images. We thank the two anonymous reviewers and the editor Fred Kucharski for the thoughtful comments and the appraisal of our manuscript. F. M. is financially supported by the China Scholarship Council with grant number 202006560002. This work uses the resources of the Deutsches Klimarechenzentrum (DKRZ) granted by its Scientific Steering Committee (WLA) under project ID bb1198.

## Author contributions

F.M. performed data analysis, created the figures, and wrote the first draft of the manuscript. S.F. conceived the concept and supervised the study. Both authors wrote and revised the manuscript.

## Funding

Open Access funding enabled and organized by Projekt DEAL.

## Competing interests

The authors declare no competing interests.

## Additional information

**Correspondence** and requests for materials should be addressed to Feifei Mu.

**Reprints and permissions information** is available at <http://www.nature.com/reprints>

**Publisher's note** Springer Nature remains neutral with regard to jurisdictional claims in published maps and institutional affiliations.

**Open Access** This article is licensed under a Creative Commons Attribution 4.0 International License, which permits use, sharing, adaptation, distribution and reproduction in any medium or format, as long as you give appropriate credit to the original author(s) and the source, provide a link to the Creative Commons licence, and indicate if changes were made. The images or other third party material in this article are included in the article's Creative Commons licence, unless indicated otherwise in a credit line to the material. If material is not included in the article's Creative Commons licence and your intended use is not permitted by statutory regulation or exceeds the permitted use, you will need to obtain permission directly from the copyright holder. To view a copy of this licence, visit <http://creativecommons.org/licenses/by/4.0/>.

© The Author(s) 2025